Anahid Khoobyar
Department of Aerospace & Mechanical Engineering, University of Southern California, USC Viterbi School of Engineering, Los Angeles, CA 90089-1453

Amin Naghdloo
Department of Aerospace & Mechanical Engineering, University of Southern California, USC Viterbi School of Engineering, Los Angeles, CA 90089-1453

Anita N. Penkova
Department of Aerospace & Mechanical Engineering, University of Southern California, USC Viterbi School of Engineering, Los Angeles, CA 90089-1453; Saban Research Institute, Children's Hospital Los Angeles, Los Angeles, CA 90027

Mark S. Humayun
Cornelius Pings Professor of Biomedical Sciences, Professor of Ophthalmology, Biomedical Engineering, and Integrative Anatomical Sciences, Director USC Ginsburg Institute for Biomedical Therapeutics, Co-Director USC Roski Eye Institute, Department of Ophthalmology, Keck School of Medicine, University of Southern California, Los Angeles, CA 90033-4682

Satwindar Singh Sadhal
Department of Aerospace & Mechanical Engineering, University of Southern California, USC Viterbi School of Engineering, Los Angeles, CA 90089-1453; Saban Research Institute, Children's Hospital Los Angeles, Los Angeles, CA 90027; Department of Ophthalmology, Keck School of Medicine, University of Southern California, Los Angeles, CA 90033-4682
e-mail: sadhal@usc.edu

Analytical and Computational Modeling of Sustained-Release Drug Implants in the Vitreous Humor

Sustained ocular drug delivery systems are necessary for patients needing regular drug therapy since frequent injection is painful, undesirable, and risky. One type of sustained-release systems includes pellets loaded with the drug, encapsulated in a porous shell that can be injected into the vitreous humor. There the released drug diffuses while the physiological flow of water provides the convective transport. The fluid flow within the vitreous is described by Darcy's equations for the analytical model and Brinkman flow for the computational analysis while the drug transport is given by the classical convection–diffusion equation. Since the timescale for the drug depletion is quite large, for the analytical model, we consider the exterior surrounding the capsule to be quasi-steady and the interior is time dependent. In the vitreous, the fluid-flow process is relatively slow, and meaningful results can be obtained for small Peclet number whereby a perturbation analysis is possible. For an isolated capsule, with approximately uniform flow in the far field around it, the mass-transfer problem requires singular perturbation with inner and outer matching. The computational model, besides accommodating the ocular geometry, allows for a fully time-dependent mass-concentration solution and also admits moderate Peclet numbers. As expected, the release rate diminishes with time as the drug depletion lowers the driving potential. The predictive results are sufficient general for a range of capsule permeability values and are useful for the design of the sustained-release microspheres as to the requisite permeability for specific drugs.
[DOI: 10.1115/1.4051785]

1 Introduction

It is estimated by the World Health Organization that about 1.3 billion people worldwide are dealing with some sort of visual impairment. There are several causes for visual impairment such as cataract, glaucoma, age-related macular degeneration, corneal opacity, diabetic retinopathy, trachoma, and refractive errors. There are a number of effective clinical approaches for treating some of these disorders, and one of the approaches is periodic delivery of the required drugs to the impaired tissue through intraocular injection. While this method is very effective, a major disadvantage is that it needs many painful injections, which is not favorable for the patients.

One approach to this problem is using implant/carrier microparticles that control drug release rate. In this regard, our effort for this work is to study analytically the sustained drug release from an injected implant in the vitreous humor (often referred to as the "vitreous"). One of the goals is to examine the role of physical parameters of both the vitreous humor and the composition of the microparticles. This work presents both analytical and numerical studies for modeling drug distribution by diffusion and convection mechanisms within the vitreous humor with the long-term goal of

[1]Corresponding author.
Contributed by the Heat Transfer Division of ASME for publication in the Journal of Heat Transfer. Manuscript received May 9, 2021; final manuscript received June 28, 2021; published online September 8, 2021. Assoc. Editor: Raj M. Manglik.

obtaining proper design values for the diffusion coefficient of microparticles and the permeability of the encapsulating membrane.

Intravitreal drug delivery is a topic of great interest [1] and in this regard predictive mathematical models for the transport processes are being developed (see discussions in Refs. [2] and [3]). There have been several past studies on ocular implants. Lee et al. [4] have provided a comprehensive review of biodegradable implants and conclude that such delivery systems offer considerable promise for treatment of ocular disease. There have been several other studies and reviews on both biodegradable and nonbiodegradable implants [5–18]. However, analytical and computational studies are few. Kim et al. [19] fabricated disk-shaped sustained-release implants, loaded with gadolinium-diethylenetriamine pentaacetic acid (Gd-DTPA) and studied experimentally the drug distribution by MRI. Additionally, they carried out a three-dimensional computer simulation of the surrogate drug distribution process. Very recently, Ferreira et al. [9] developed a computational model for a disk-shaped intravitreal implant.

Our approach consists of analytical modeling by singular perturbation for low Peclet numbers and computational modeling for low-to-moderate Peclet numbers. For the analytical model, the vitreous is modeled as a Darcy fluid and the localized flow in the vicinity of the implanted capsule is taken to be uniform flow. For the computational analysis, the geometry is taken to be closer to that of the human eye, and the flow field within the vitreous is described by Brinkman's equations for the porous medium. We first begin with the singular perturbation approach.

2 Mathematical Model: Singular Perturbation Analysis

We consider a spherical capsule of radius R placed in the vitreous humor where the fluid flow is assumed to be described by Darcy's equation for a porous medium. This is reasonable because the vitreous, while in a gelatinous state, consists of a 99.9% liquid in a fibrous mesh of hyaluronic acid and collagen [20,21]. While the fluid flow field in the vitreous has a distribution, we consider a small capsule and approximate the flow in the vicinity as a uniform field perturbed by the presence of the particle. This is described graphically in Figs. 1 and 2. The differential equations for fluid flow in dimensional form are given next.

2.1 Differential Equations. We adopt an axisymmetric spherical coordinate system (r^*, θ) with the localized uniform flow in the z^* direction.

2.1.1 Fluid Flow. The momentum- and mass-conservation equations with the Darcy flow approximation are given by

$$\boldsymbol{u}^* = -\frac{K}{\mu}\nabla^* p^*, \ \nabla^{*2} p^* = 0 \tag{1}$$

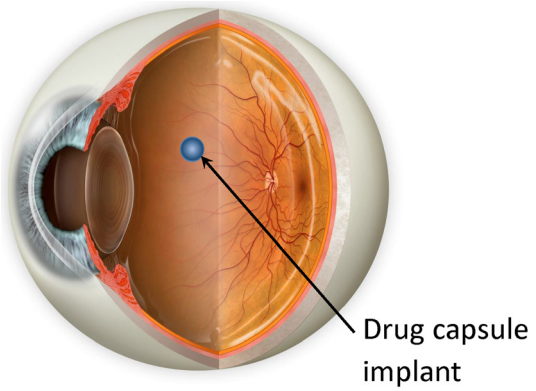

Fig. 1 Spherical drug implant in the vitreous (not to scale)

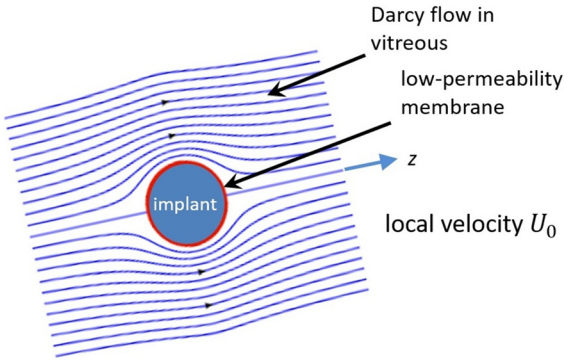

Fig. 2 Local flow around the spherical implant in the vitreous

where $\boldsymbol{u}^*$ is the velocity field, p^* is the pressure, K is the Darcy coefficient, and μ is the viscosity of the liquid part of the vitreous.

2.1.2 Mass Transfer. The mass transfer in the exterior is described by the convection-diffusion equation for the drug concentration c^*

$$\frac{\partial c^*}{\partial t^*} + \boldsymbol{u}^* \cdot \nabla^* c^* = D\nabla^{*2} c^* \tag{2}$$

where D is the diffusion coefficient for the drug in the vitreous. For the perturbation analysis, the quasi-steady approximation for the exterior mass flow is made whereby the time-derivative term is dropped. Considering that the drug release is, by design, slow, we assume that the released drug quickly reaches a steady-state in the timescale of the capsule lifetime. This is the basis of the analytical model. However, in the computational model, the time-derivative term is kept. In the interior of the capsule, we assume no convective transport, and pure diffusion describes the mass flow, i.e.,

$$\frac{\partial \widehat{c}^*}{\partial t^*} = \widehat{D}\nabla^{*2}\widehat{c}^* \tag{3}$$

where $\widehat{D}$ is the diffusion coefficient of the drug in the encapsulated liquid–drug solution, and $\widehat{c}^*$ is the drug concentration there. The initial and boundary/interface conditions are given next.

2.2 Initial and Boundary/Interface Conditions

2.2.1 Flow Field. The far-field velocity is taken to be U_0 so that

$$\boldsymbol{u}^*|_{r^*\to\infty} = U_0\widehat{\boldsymbol{e}}_z \tag{4}$$

where r^* is the spherical radial distance from the center of the implant, and $\widehat{\boldsymbol{e}}_z$ is a unit vector in the direction of flow. At the surface of the capsule, zero normal velocity is applied, i.e.,

$$\boldsymbol{u}^* \cdot \boldsymbol{n}\,|_{r^*=R} = 0 \tag{5}$$

where $\boldsymbol{n}$ is a unit normal vector. Here, the zero tangential velocity condition cannot be satisfied since the differential-equation system is second-order, and we tolerate slip at the interface.

2.2.2 Mass Transfer. The initial drug concentration is taken to be c_0 in the capsule and zero outside so that

$$\widehat{c}^*|_{t^*=0} = c_0 \tag{6}$$

and

$$c^*|_{t^*=0} = 0 \tag{7}$$

The concentration far away from the capsule is taken to be zero, i.e.,

$$c^*|_{r^*\to\infty} = 0 \tag{8}$$

At the interface $r^* = R$, we have continuity of mass flux but the concentration is allowed to have a jump across the membrane. These conditions are described by

$$-\widehat{D}\left.\frac{\partial \widehat{c}^*}{\partial r^*}\right|_{r^*=R} = -D\left.\frac{\partial c^*}{\partial r^*}\right|_{r^*=R} = l(\widehat{c}^* - c^*)|_{r^*=R} \tag{9}$$

where l is the interfacial mass-transfer coefficient representing membrane permeability. It should be noted in this mathematical model where the vitreous humor region is approximated as an infinite medium, the initial condition (7) and the boundary condition (8) are taken to be the same for compatibility.

2.3 Nondimensional Scaling of the Transport Equations. To render the equations dimensionless, we apply the following dimensionless scaling:

$$r = \frac{r^*}{R}, \quad \nabla = R\nabla^*, \quad z = \frac{z^*}{R}, \quad P = \frac{p^* KR}{U_0\mu}$$

$$c = \frac{c^*}{c_0}, \quad \widehat{c} = \frac{\widehat{c}^*}{c_0}, \quad \mathrm{Pe} = \frac{U_0 R}{D} = \varepsilon \ll 1$$

$$\mathrm{Bi} = \frac{lR}{D} \ll 1, \quad \phi_D = \frac{\widehat{D}}{D}, \quad \Phi_D = \phi_D\left(1 + \frac{1}{\mathrm{Bi}}\right), \quad \mathrm{Sh} = \frac{Q}{4\pi RD},$$
$$\mathrm{Fo} = t = \frac{t^*\widehat{D}}{R^2}, \quad \Psi_D = \phi_D\left(\frac{1}{2} + \frac{1}{\mathrm{Bi}}\right)$$

where Q represents the total mass transport rate from the capsule, and Bi, Pe, Sh, and Fo are the Biot, Peclet, Sherwood, and Fourier numbers. The Biot number is defined with the continuous phase diffusion coefficient because it makes the definition of the parameters Φ_D and Ψ_D a bit less cumbersome. With this scaling, Eqs. (1)–(9) take the following dimensionless form:

Darcy flow

$$\boldsymbol{u} = -\nabla P, \quad \nabla^2 P = 0 \tag{10}$$

Exterior mass transfer

$$\varepsilon\,\boldsymbol{u}\cdot\nabla c = \nabla^2 c \tag{11}$$

where, for the analytical solution, the time-derivative term has been dropped under the quasi-steady approximation.

Interior mass transfer

$$\frac{\partial \widehat{c}}{\partial t} = \nabla^2 \widehat{c} \tag{12}$$

Initial, boundary, and interface conditions

$$t = 0 : \widehat{c} = 1, \quad c = 0 \tag{13}$$

$$r \to 0 : \widehat{c} < \infty \tag{14}$$

$$r = 1 : \boldsymbol{u}\cdot\boldsymbol{n} = 0, \quad -\phi_D\frac{\partial \widehat{c}}{\partial r} = -\frac{\partial c}{\partial r} = \mathrm{Bi}(\widehat{c} - c) \tag{15}$$

$$r \to \infty : \boldsymbol{u} \to \boldsymbol{e}_z, c \to 0 \tag{16}$$

2.4 Analytical Solution

2.4.1 Velocity and Pressure Fields. Equations (10) with velocity boundary conditions (15) and (16) represent the standard potential flow past a sphere. The pressure field representing the velocity potential is found to be the following in a spherical coordinate system:

$$P = -\left(r - \frac{1}{2r^2}\right)\bar{\mu} \tag{17}$$

where $\bar{\mu} = \cos\theta$. The gradient of the pressure gives the velocity field with the following components

$$u_r = -\frac{\partial p}{\partial r} = \left(1 - \frac{1}{r^3}\right)\bar{\mu} \tag{18}$$

$$u_\theta = -\frac{1}{r}\frac{\partial p}{\partial \theta} = -\left(1 + \frac{1}{2r^3}\right)\left(1 - \bar{\mu}^2\right)^{1/2} \tag{19}$$

2.4.2 Concentration Fields. As mentioned earlier, the interior of the capsule is time-dependent diffusion-only based transport while the exterior in quasi-steady with low Pe convection and diffusion. We use the method of Laplace transform and begin by transforming Eqs. (11)–(15). We define the transforms of the concentrations fields as

$$\mathcal{L}\widehat{c}(r,t,\mu) = \bar{\widehat{c}}(r,\bar{\mu},s), \text{and} \mathcal{L}c(r,\,t,\bar{\mu}) = \bar{c}(r,\bar{\mu},s) \tag{20}$$

where

$$\mathcal{L}[f(t)] = \int_0^\infty e^{-st} f(t)\,dt = \bar{f}(s) \tag{21}$$

Under the transform, and the expressions (18) and (19) for the velocity components, Eqs. (11) and (12) become

$$\frac{\partial^2 \bar{c}}{\partial r^2} + \frac{2}{r}\frac{\partial \bar{c}}{\partial r} + \frac{1}{r^2}\frac{\partial}{\partial \bar{\mu}}\left[\left(1 - \bar{\mu}^2\right)\frac{\partial \bar{c}}{\partial \mu}\right] = \varepsilon\left[\left(1 - \frac{1}{r^3}\right)\bar{\mu}\frac{\partial \bar{c}}{\partial r} + \frac{\left(1 - \bar{\mu}^2\right)}{r^2}\left(1 + \frac{2}{r^3}\right)\frac{\partial \bar{c}}{\partial \bar{\mu}}\right] \tag{22}$$

and

$$\frac{\partial^2 \bar{\widehat{c}}}{\partial r^2} + \frac{2}{r}\frac{\partial \bar{\widehat{c}}}{\partial r} + \frac{1}{r^2}\frac{\partial}{\partial \bar{\mu}}\left[\left(1 - \bar{\mu}^2\right)\frac{\partial \bar{\widehat{c}}}{\partial \mu}\right] = s\bar{\widehat{c}} - 1 \tag{23}$$

respectively. The initial condition (13) gets imbedded in Eqs. (22) and (23). The boundary and interface conditions (14)–(16) change only in notation, i.e.,

$$r \to 0 : \bar{\widehat{c}} < \infty \tag{24}$$

$$r = 1 \quad -\phi_D\frac{\partial \bar{\widehat{c}}}{\partial r} = -\frac{\partial \bar{c}}{\partial r} = Bi(\bar{\widehat{c}} - \bar{c}) \tag{25}$$

$$r \to \infty : \bar{c} \to 0 \tag{26}$$

2.4.3 Solution by Singular Perturbation. The singular perturbation method has been successfully applied to heat and mass transfer problems pertaining to isolated spherical and nonspherical particles experiencing convective and diffusive transport [22–28]. Following the procedures developed in classical works by Acrivos and Taylor [26], Gupalo and Ryazantsev [27], and more recently by Bell et al. [28] for fully steady-state cases, we extend the

technique for the transient interior (see Sadhal [29]). However, we appropriately apply the Darcy velocity field instead of Stokes flow in the vitreous humor region. Thus, we apply the expansions for $\mathrm{Pe} = \varepsilon \ll 1$ so that

$$\bar{\hat{c}} = \hat{h}_0 + \varepsilon\hat{h}_1 + \varepsilon^2\hat{h}_2 + \cdots \tag{27}$$

$$\bar{c} = h_0 + \varepsilon h_1 + \varepsilon^2 h_2 + \cdots \tag{28}$$

This leads to the following hierarchy of problems where a spherical coordinate system is employed. The development relies on an earlier work by Sadhal [29] but as mentioned, the flow field in the present case is different and most importantly, we have taken the current perturbation analysis to $O(\varepsilon^2)$.

Order ε^0

The exterior problem to the leading order is

$$\frac{\partial^2 h_0}{\partial r^2} + \frac{2}{r}\frac{\partial h_0}{\partial r} + \frac{1}{r^2}\frac{\partial}{\partial \bar{\mu}}\left[\left(1-\bar{\mu}^2\right)\frac{\partial h_0}{\partial \bar{\mu}}\right] = 0 \tag{29}$$

and the interior problem satisfies

$$\frac{\partial^2 \hat{h}_0}{\partial r^2} + \frac{2}{r}\frac{\partial \hat{h}_0}{\partial r} + \frac{1}{r^2}\frac{\partial}{\partial \bar{\mu}}\left[\left(1-\bar{\mu}^2\right)\frac{\partial \hat{h}_0}{\partial \mu}\right] = s\hat{h}_0 - 1 \tag{30}$$

with boundary and interface conditions

$$r \to 0 : \hat{h}_0 < \infty \tag{31}$$

$$r = 1 : -\phi_D \frac{\partial \hat{h}_0}{\partial r} = -\frac{\partial h_0}{\partial r} = Bi\left(\hat{h}_0 - h_0\right) \tag{32}$$

$$r \to \infty : h_0 \to 0 \tag{33}$$

The general solutions for Eqs. (27) and (28) are

$$h_0(r,\bar{\mu},s) = \sum_{n=0}^{\infty}\left[A_n(s)r^{-(n+1)} + B_n(s)r^n\right]P_n(\bar{\mu}) \tag{34}$$

and

$$\hat{h}_0(r,\bar{\mu},s) = \sum_{n=0}^{\infty}\left[\hat{A}_n(s)i_n(qr) + \hat{B}_n(s)k_n(qr)\right]P_n(\bar{\mu}) + \frac{1}{s} \tag{35}$$

where $P_n(\bar{\mu})$ represents Legendre polynomials, $\bar{\mu} = \cos\theta$ $q = s^{1/2}$, and $i_n(qr)$ and $k_n(qr)$ are spherical Bessel functions with

$$i_0(qr) = \frac{\sinh qr}{qr} \quad \text{and} \quad i_1(qr) = -\frac{\sinh qr}{(qr)^2} + \frac{\cosh qr}{qr} \tag{36}$$

Upon satisfying (31)–(33), we obtain

$$A_0(s) = \frac{\phi_D(q\cosh q - \sinh q)}{s\{(1-\Phi_D)\sinh q - \Phi_D\, q\cosh q\}} \tag{37}$$

$$\hat{A}_0(s) = \frac{q}{s\{(1-\Phi_D)\sinh q - \Phi_D\, q\cosh q\}} \tag{38}$$

$$A_n(s) = \hat{A}_0(s) = 0, \quad n \geq 1 \tag{39}$$

and

$$B_n(s) = \hat{B}_0(s) = 0, \quad n \geq 0 \tag{40}$$

resulting in just a spherically symmetric leading order

$$h_0(r,\bar{\mu},s) = \frac{A_0(s)}{r}, \quad \hat{h}_0(r,\bar{\mu},s) = \hat{A}_0(s)\frac{\sinh(qr)}{qr} + \frac{1}{s} \tag{41}$$

The constants ϕ_D and Φ_D are related to the mass-transfer Biot number, Bi, and have been defined at the beginning of Sec. 2.3. We shall invert to the time domain after obtaining higher order solutions.

Order ε^1

The exterior problem to this order is

$$\frac{\partial^2 h_1}{\partial r^2} + \frac{2}{r}\frac{\partial h_1}{\partial r} + \frac{1}{r^2}\frac{\partial}{\partial \bar{\mu}}\left[\left(1-\bar{\mu}^2\right)\frac{\partial h_1}{\partial \bar{\mu}}\right] = -\frac{A_0(s)}{r^2}\left(1 - \frac{1}{r^3}\right)\mu \tag{42}$$

while the interior problem is

$$\frac{\partial^2 \hat{h}_1}{\partial r^2} + \frac{2}{r}\frac{\partial \hat{h}_1}{\partial r} + \frac{1}{r^2}\frac{\partial}{\partial \bar{\mu}}\left[\left(1-\mu^2\right)\frac{\partial \hat{h}_1}{\partial \bar{\mu}}\right] = s\hat{h}_1 \tag{43}$$

with boundary and interface conditions

$$r \to 0 : \hat{h}_1 < \infty \tag{44}$$

$$r = 1 : -\phi_D \frac{\partial \hat{h}_1}{\partial r} = -\frac{\partial h_1}{\partial r} = Bi\left(\hat{h}_1 - h_1\right) \tag{45}$$

$$r \to \infty : h_1 \to 0 \tag{46}$$

The general solutions for Eqs. (42) and (43) are

$$h_1(r,\bar{\mu},s) = \sum_{n=0}^{\infty}\left[A_n^*(s)r^{-(n+1)} + B_n^*(s)r^n\right]P_n(\bar{\mu}) + A_0(s)\left(\frac{1}{2} - \frac{1}{4r^3}\right)\bar{\mu} \tag{47}$$

and

$$\hat{h}_1(r,\bar{\mu},s) = \sum_{n=0}^{\infty}\left[\hat{A}_n^*(s)i_n(qr) + \hat{B}_n^*(s)k_n(qr)\right]P_n(\bar{\mu}) \tag{48}$$

The exterior solution given by Eq. (47) does not vanish as $r \to \infty$ and the problem is therefore singular. To handle this, we setup the outer problem using the outer variable $\rho = \varepsilon r$ and the dependent variable as $\bar{c}(r,\mu,s) = \bar{C}(\rho,\mu,s)$. In terms of ρ, the exterior region Eq. (22) becomes

$$\frac{\partial^2 H}{\partial \rho^2} + \frac{2}{\rho}\frac{\partial H}{\partial \rho} + \frac{1}{\rho^2}\frac{\partial}{\partial \bar{\mu}}\left[\left(1-\bar{\mu}^2\right)\frac{\partial H}{\partial \mu}\right] = \left[\left(1 - \frac{\varepsilon^3}{\rho^3}\right)\bar{\mu}\frac{\partial H}{\partial \rho} + \frac{\left(1-\bar{\mu}^2\right)}{\rho}\left(1 + \frac{2\varepsilon^3}{\rho^3}\right)\frac{\partial H}{\partial \bar{\mu}}\right] \tag{49}$$

We now setup the outer expansion of the exterior region in the form

$$\bar{C}(\rho,\mu,s) = \sum_{n=0}^{\infty} g_n(\varepsilon)H_n \tag{50}$$

where $g_n(\varepsilon)$ will be determined by inner and outer matching in the exterior region. For the leading order in of this expansion, it is reasonable and not difficult to show that [26]

$$\frac{\partial^2 H_0}{\partial \rho^2}+\frac{2}{\rho}\frac{\partial H_0}{\partial \rho}+\frac{1}{\rho^2}\frac{\partial}{\partial \bar{\mu}}\left[\left(1-\bar{\mu}^2\right)\frac{\partial H_0}{\partial \bar{\mu}}\right] = \left[\bar{\mu}\frac{\partial H_0}{\partial \rho}+\frac{\left(1-\bar{\mu}^2\right)}{\rho}\frac{\partial H_0}{\partial \bar{\mu}}\right] \tag{51}$$

The solution to this is

$$H_0(\rho,\mu,s)=e^{\rho\mu/2}\sum_{n=0}^{\infty}C_n(s)k_n\left(\frac{\rho}{2}\right)P_n(\mu) \tag{52}$$

where $k_n\left(\frac{\rho}{2}\right)$ represents spherical Bessel functions. Now satisfying the boundary/interface conditions (44) and (45) for h_1 and matching

$$h_0+\varepsilon h_1=g_0(\varepsilon)H_0 \tag{53}$$

to $O(\varepsilon)$, while skipping the tedious algebra, yields

$$C_0(s)=\frac{1}{2}A_0(s),\quad B_0^*=-\frac{1}{2}A_0(s),\quad g_0(\varepsilon)=\varepsilon \tag{54}$$

$$A_0^*(s)=\frac{1}{2s}\left(\frac{\phi_D(q\cosh q-\sinh q)}{\left\{(1-\Phi_D)\sinh q-\Phi_D\, q\cosh q\right\}}\right)^2 \tag{55}$$

$$\widehat{A}_0^*(s)=-\frac{q\phi_D(q\cosh q-\sinh q)}{2s\left\{(1-\Phi_D)\sinh q-\Phi_D\, q\cosh q\right\}^2} \tag{56}$$

$$\widehat{A}_1^*(s)=-\frac{\frac{5}{8}A_0(s)}{(1-2\Psi_D)(q\cosh q-\sinh q)+\Psi_D q^2\sinh q} \tag{57}$$

where $\Psi_D=\phi_D\left(\frac{1}{2}+1/\mathrm{Bi}\right)$ has been defined at the beginning of Sec. 2.3. Keeping only the nonzero terms, Eqs. (47) and (48) may be written as

$$h_1=\frac{A_0^*(s)}{r}--\frac{1}{2}A_0(s)+\left[A_0(s)\left(\frac{1}{2}-\frac{1}{4r^3}\right)\right]\bar{\mu} \tag{58}$$

$$\widehat{h}_1=\widehat{A}_0^*(s)\frac{\sinh qr}{qr}+\widehat{A}_1^*(s)\left(-\frac{\sinh qr}{q^2r^2}+\frac{\cosh qr}{qr}\right)\bar{\mu} \tag{59}$$

and the outer solution is

$$H_0=A_0(s)\frac{e^{-\rho(1-\bar{\mu})/2}}{\rho} \tag{60}$$

We can now go to the next order.

Order ε^2

In the exterior region

$$\frac{\partial^2 h_2}{\partial r^2}+\frac{2}{r}\frac{\partial h_2}{\partial r}+\frac{1}{r^2}\frac{\partial}{\partial \bar{\mu}}\left[\left(1-\bar{\mu}^2\right)\frac{\partial h_2}{\partial \bar{\mu}}\right] = \left(1-\frac{1}{r^3}\right)\bar{\mu}\frac{\partial h_1}{\partial r}+\left(1+\frac{2}{r^3}\right)\frac{\left(1-\bar{\mu}^2\right)}{r}\frac{\partial h_1}{\partial \bar{\mu}} = \sum_{k=0}^{2}Z_k(r)P_k(\bar{\mu}) \tag{61}$$

where

$$Z_0(r)=\frac{A_0(s)}{3r}+\frac{A_0(s)}{4r^2}+\frac{A_1^*(s)}{r^6}-\frac{A_0(s)}{3r^7} \tag{62}$$

$$Z_1(r)=-A_0^*(s)\left(\frac{1}{r^2}-\frac{1}{r^5}\right) \tag{63}$$

$$Z_2(r)=-\frac{A_0(s)}{3r}-\frac{2A_1^*(s)}{r^3}+\frac{A_0(s)}{2r^4}+\frac{A_1^*(s)}{r^6}-\frac{5A_0(s)}{12r^7} \tag{64}$$

Within the capsule

$$\frac{\partial^2 \widehat{h}_2}{\partial r^2}+\frac{2}{r}\frac{\partial \widehat{h}_2}{\partial r}+\frac{1}{r^2}\frac{\partial}{\partial \bar{\mu}}\left[\left(1-\bar{\mu}^2\right)\frac{\partial \widehat{h}_2}{\partial \bar{\mu}}\right]=s\widehat{h}_2 \tag{65}$$

The boundary and interface conditions remain the same as for $O(\varepsilon)$, i.e.,

$$r\to 0:\widehat{h}_2<\infty \tag{66}$$

$$r=1:-\phi_D\frac{\partial \widehat{h}_2}{\partial r}=-\frac{\partial h_2}{\partial r}=Bi\left(\widehat{h}_2-h_2\right) \tag{67}$$

$$r\to\infty:h_2\to 0 \tag{68}$$

The general solutions for Eqs. (61) and (65) are

$$h_2(r,\mu,s)=\sum_{n=0}^{\infty}L_k(r)P_n(\bar{\mu}) \tag{69}$$

where

$$L_0(r)=-A_0\left(\frac{1}{120r^5}+\frac{1}{24r^2}-\frac{1}{6}r\right)-\frac{A_1^*}{36r^4}+\frac{a_0}{r}+b_0 \tag{70}$$

$$L_1(r)=A_0\left(\frac{1}{4r^3}+\frac{1}{2}\right)+\frac{a_1}{r^2}+b_1 r \tag{71}$$

$$L_2(r)=-A_0\left(\frac{1}{24r^5}+\frac{5}{24r^2}-\frac{1}{6}r\right)+\frac{A_1^*}{3r}+\frac{a_2}{r^3}+b_2r^2 \tag{72}$$

$$L_k(r)=\left(\frac{a_k}{r^{k+1}}+b_k r^k\right),\quad k\geq 3 \tag{73}$$

and

$$\widehat{h}_2(r,\mu,s)=\sum_{n=0}^{\infty}\left[F_n^*(s)i_n(qr)+E_n^*(s)k_n(qr)\right]P_n(\bar{\mu}) \tag{74}$$

In the outer region, the differential equation is the same as Eq. (51), i.e.,

$$\frac{\partial^2 H_1}{\partial \rho^2}+\frac{2}{\rho}\frac{\partial H_1}{\partial \rho}+\frac{1}{\rho^2}\frac{\partial}{\partial \bar{\mu}}\left[\left(1-\mu^2\right)\frac{\partial H_1}{\partial \bar{\mu}}\right] = \left[\mu\frac{\partial H_1}{\partial \rho}+\frac{\left(1-\bar{\mu}^2\right)}{\rho}\frac{\partial H_1}{\partial \bar{\mu}}\right] \tag{75}$$

with the solution

$$H_1(\rho,\mu,s)=e^{\rho\bar{\mu}/2}\sum_{n=0}^{\infty}C_n^*(s)k_n\left(\frac{\rho}{2}\right)P_n(\bar{\mu}) \tag{76}$$

Once again, we see that the far-field condition (85) cannot be satisfied, and asymptotic matching is needed. Now, satisfying the

remaining conditions (66) and (67) carrying out the matching to $O(\varepsilon^2)$

$$h_0 + \varepsilon h_1 + \varepsilon^2 h_2 = g_0(\varepsilon)H_0 + g_1(\varepsilon)H_1, \quad (g_0(\varepsilon) = \varepsilon) \tag{77}$$

we obtain

$$a_0(s) = -\phi_D F_0^* \dot{i}_0(q)q + \frac{3}{16}A_0 + \frac{1}{3}A_1^* \tag{78}$$

$$b_0(s) = -\frac{1}{2}a_0(s) \tag{79}$$

$$F_0^*(s) = \frac{\frac{11}{40}A_0 - \frac{1}{12}A_1^*}{i_0(q) + \Psi_D \dot{i}_0(q)q} \tag{80}$$

and $g_1(\varepsilon)$ is identified as ε^2. Some of the other constants are as follows:

$$a_k = b_k = 0,\ k \geq 3, \quad b_2 = 0,\ E_n^* = 0,\ n \geq 0 \tag{81}$$

Other constants $[a_2, F_1^*, F_2^*,]$, pertaining to the $P_1(\mu)$ and $P_2(\mu)$, have been found but are not reported here because these are not needed for the total mass transfer which is calculated next. Also, the inversion to the time domain will be carried out at that stage.

2.4.4 Total Mass Transfer. The total mass transfer in the Laplace domain is given by

$$-\phi_D \frac{\partial \bar{\hat{c}}}{\partial r}\bigg|_{r=1} = \bar{\mathrm{Sh}}_0(s) + \varepsilon \bar{\mathrm{Sh}}_1(s) + \varepsilon^2 \bar{\mathrm{Sh}}_2(s) + \cdots \tag{82}$$

where the Sherwood number expansion terms are

$$\bar{\mathrm{Sh}}_0(s) = A_0(s), \quad \bar{\mathrm{Sh}}_1(s) = A_0^*(s) \tag{83}$$

and

$$\bar{\mathrm{Sh}}_2(s) = -\phi_D F_0^*(s) q i_0'(q) \tag{84}$$

The next step is inversion into the time domain using the Mellin integral

$$\mathrm{Sh}(t) = \frac{1}{2\pi i}\int_{\gamma - i\infty}^{\gamma + i\infty} \bar{\mathrm{Sh}}(s)e^{st}\, ds \tag{85}$$

This is a fairly elaborate procedure entailing first-order and second-order poles in the complex domain. We give only the results. Thus

$$\mathrm{Sh}_0(t) = 2\phi_D \sum_{n=1}^{\infty} \frac{e^{-\lambda_n^2 t}}{1 - \Phi_D + \Phi_D^2 \lambda_n^2} \tag{86}$$

and

$$\mathrm{Sh}_1(t) = \phi_D^2 \sum_{n=1}^{\infty} \frac{e^{-\lambda_n^2 t}}{G_n^2}\left[\left(1 - \Phi_D - \Phi_D^2\lambda_n^2\right) - \frac{2\left(1 - \Phi_D\lambda_n^2 + \lambda_n^2 t\right)}{G_n}\right] \tag{87}$$

where

$$G_n = 1 - \Phi_D + \Phi_D^2 \lambda_n^2 \tag{88}$$

and λ_n is the set of roots of the transcendental equation

$$(1 - \Phi_D)\tan\lambda_n = -\Phi_D \lambda_n,\ n = 1, 2, 3, \ldots \tag{89}$$

The $O(\varepsilon^2)$ term of the Sherwood number is an elaborate expression that has five parts with contributions from three sets of poles from the expressions in the Laplace domain. We express $\mathrm{Sh}_2(t)$ as

$$\mathrm{Sh}_2(t) = \left[\frac{39}{80} + \frac{5}{96\eta}\right]\mathrm{Sh}_0(t) + q_a^{\delta}(t) + q_b^{\delta}(t) + q_b^{\lambda}(t) + q_b^{\beta}(t) \tag{90}$$

where $\eta = 1/Bi + \frac{1}{2}$,

$$q_a^{\delta}(t) = -\left[\frac{39}{80} + \frac{5}{96\eta}\right]\sum_{n=1}^{\infty} \frac{2\phi_D e^{-\delta_n^2 t}}{1 - \Psi_D + \Psi_D^2 \delta_n^2} \tag{91}$$

$$q_b^{\delta}(t) = \frac{5\phi_D}{48\eta}\sum_{n=1}^{\infty} \frac{e^{-\delta_n^2 t}}{(1 - 2\Psi_D + \Psi_D^2\delta_n^2)(1 - \Psi_D + \Psi_D^2\delta_n^2)} \tag{92}$$

$$q_b^{\lambda}(t) = \frac{5\phi_D}{96\eta}\sum_{n=1}^{\infty} \frac{e^{-\lambda_n^2 t}}{(1 - \Phi_D - \Phi_D^2\lambda_n^2)(1 - 2\Psi_D + \Psi_D^2\lambda_n^2)} \tag{93}$$

and

$$q_b^{\beta}(t) = +\frac{5}{96}\sum_{n=1}^{\infty} \frac{\phi_D^3 \Psi_D^2 \beta_n^4 e^{-\beta_n^2 t}}{[1 + \Psi_D - \Psi_D^2(2 - \beta_n^2)](1 - 2\Psi_D + \Psi_D\Phi_D\beta_n^2)(1 - 2\Psi_D + \Psi_D^2\beta_n^2)} \tag{94}$$

The λ_n values have been defined in Eq. (89) and δ_n, and β_n are the roots of the transcendental equations

$$(1 - \Psi_D)\tan\delta_n = -\Psi_D \delta_n \tag{95}$$

and

$$\tan\beta_n = \frac{\beta_n(1 - 2\Psi_D)}{1 - 2\Psi_D + \Psi_D\beta_n^2} \tag{96}$$

The Sherwood number can be readily computed from these expressions. Since these are limiting results for $\mathrm{Pe} \ll 1$, we shall combine these results with the numerical analysis where proper comparison of the two models (perturbation analysis and computational) can be made.

Besides the mass depletion rate expressed by the Sherwood number, there is also interest in how much of the drug remains in the capsule as a function of time. This can be represented by the volumetric average in capsule.

2.4.5 Average Capsule Concentration. Using the expansion for $\bar{\hat{c}}(r, \mu, s)$ as given by Eq. (27) and using the expressions for $\hat{h}_0$, $\hat{h}_1$ and $\hat{h}_2$ as given by Eqs. (41), (48), and (74), the terms independent of $\bar{\mu}$ can be volume-integrated to give a spatial average of

$\bar{\bar{c}}(r,\mu,s)$ in the Laplace domain. Inversion into the time domain gives

$$\widehat{C}_{avg}(t) = \widehat{C}_0(t) + \varepsilon\widehat{C}_1(t) + \varepsilon^2\widehat{C}_2(t) + \cdots \tag{97}$$

where

$$\widehat{C}_0(t) = 6\sum_{n=1}^{\infty}\frac{e^{\lambda_n^2 t}}{G_n\lambda_n^2} \tag{98}$$

$$\widehat{C}_1(t) = 3\phi_D\sum_{n=1}^{\infty}\frac{e^{-\lambda_n^2 t}}{G_n^2\lambda_n^2}\left[\left(1-\Phi_D-\Phi_D^2\lambda_n^2\right) - \frac{2\left(2-\Phi_D\lambda_n^2+\lambda_n^2 t\right)}{G_n}\right] \tag{99}$$

$$\widehat{C}_2(t) = +\left[\frac{39}{80}+\frac{5}{96\eta}\right]\widehat{C}_0(t) + c_a^{\delta}(t) + c_b^{\delta}(t) + c_b^{\lambda}(t) + c_b^{\beta}(t) \tag{100}$$

with

$$c_a^{\delta}(t) = -\left[\frac{39}{80}+\frac{5}{96\eta}\right]\sum_{n=1}^{\infty}\frac{6e^{-\delta_n^2 t}}{\left(1-\Psi_D+\Psi_D^2\delta_n^2\right)\delta_n^2} \tag{101}$$

$$c_b^{\delta}(t) = \frac{5}{16\eta}\sum_{n=1}^{\infty}\frac{e^{-\delta_n^2 t}}{(1-2\Psi_D+\Psi_D^2\delta_n^2)(1-\Psi_D+\Psi_D^2\delta_n^2)\delta_n^2} \tag{102}$$

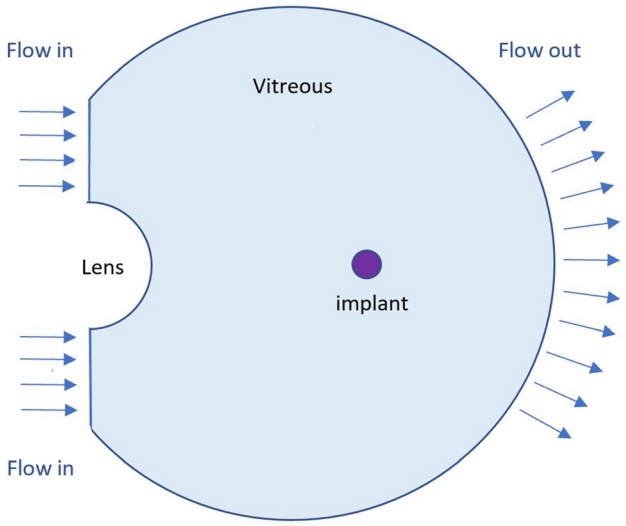

Fig. 3 Schematic of the computational domain with inlet–outlet flow characterization

$$c_b^{\lambda}(t) = \frac{5}{32\eta}\sum_{n=1}^{\infty}\frac{e^{-\lambda_n^2 t}}{(1-\Phi_D-\Phi_D^2\lambda_n^2)(1-2\Psi_D+\Psi_D^2\lambda_n^2)\lambda_n^2} \tag{103}$$

$$c_b^{\beta}(t) = \frac{5}{32}\sum_{n=1}^{\infty}\frac{\phi_D^2\Psi_D^2\beta_n^2 e^{-\beta_n^2 t}}{[1+\Psi_D-\Psi_D^2(2-\beta_n^2)](1-2\Psi_D+\Psi_D\Phi_D\beta_n^2)(1-2\Psi_D+\Psi_D^2\beta_n^2)} \tag{104}$$

As with the Sherwood number expressions, λ_n, δ_n, and β_n are the roots of the transcendental equations given by Eqs. (89), (95), and (96). In the limit of $\mathrm{Bi} \ll 1$, one can approximate the capsule concentration to be uniform, and simple mass-transfer analysis yields

$$\mathrm{Sh}(t) = b\left\{1+\frac{1}{2}\varepsilon b\left(1-\frac{3bt}{\phi_D}\right)\right\}e^{-\frac{3bt}{\phi_D}}, \quad \text{where} \quad b = \frac{\mathrm{Bi}}{1+\mathrm{Bi}} \tag{105}$$

This result is based on the $O(\varepsilon)$ solution and of course limited by $\varepsilon \ll 1$. It can be used to calculate the capsule half-life to that order which is given in the Conclusions section.

The numerical results from this perturbational analysis will be provided along with those from the computational analysis that we treat next.

3 Computational Analysis

The computational analysis for the model was carried out by a finite element scheme that allowed accommodation for the eye geometry and the corresponding boundary conditions pertaining to eye physiology.

3.1 Geometry. The computational finite element model is based on three-dimensional axisymmetric geometry as given in Fig. 3. Since the goal is to model the flow inside the vitreous humor, the overall geometry is assumed to be a spherical segment with a partial cut on the region where vitreous is in contact with that ciliary body and the lens. The detailed dimensions together with boundary and domain annotations are presented in Fig. 3. The Petrov–Galerkin method was used with the finite element meshes illustrated in Figs. 4 and 5.

3.2 Assumptions. As mentioned before, the goal of this study is to model the physiological intraocular flow as well as the transport phenomenon associated with a drug implant. In this regard,

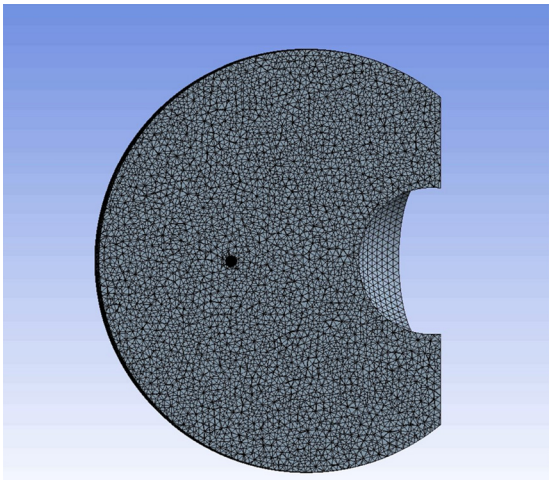

Fig. 4 A sectional schematic of the finite element meshwork in the vitreous region

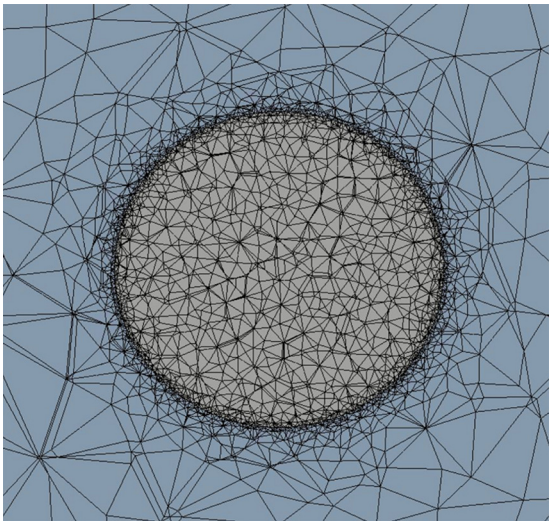

Fig. 5 A schematic of the meshwork in the spherical implant

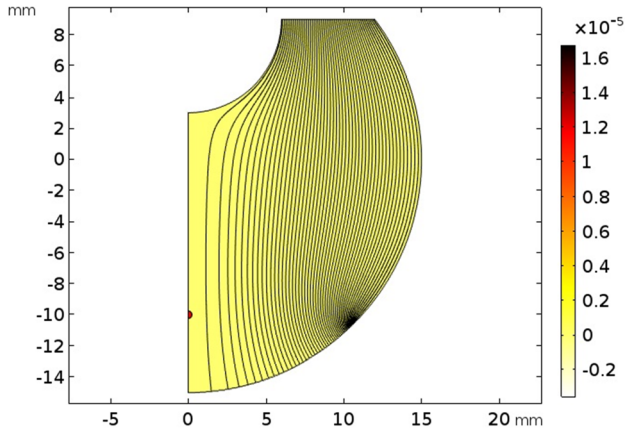

Fig. 6 Flow streamlines for the computational model

Table 1 Initial, boundary, and interface conditions

	Flow (Br)	Concentration
Inlet	$-\boldsymbol{u}^* \cdot \boldsymbol{n} = u_0$	$-\boldsymbol{n} \cdot (-D\nabla^* c^* + \boldsymbol{u}^* c^*) = l_i(0 - c^*)$
Outlet	$p^* = 0$	$\boldsymbol{n} \cdot (-D\nabla^* c^* + \boldsymbol{u}^* c^*) = l_o(c^* - 0)$
Wall	$\boldsymbol{u}^* = \boldsymbol{0}$	$\boldsymbol{n} \cdot (-D\nabla^* c^* + \boldsymbol{u}^* c^*) = 0$
Capsule	$\boldsymbol{u}^* = \boldsymbol{0}$	$-\boldsymbol{n} \cdot \widehat{D}\nabla^* \widehat{c}^* = -\boldsymbol{n} \cdot D\nabla^* c^* = l(\widehat{c}^* - c^*)$
$t^* = 0$	—	$\widehat{c}^* = c_0,\ c^* = 0$

two mathematical models are used and each of them requires a set of simplifying assumptions. Of those, we have already conducted the calculations for the Pe $\ll 1$ with Darcy flow in the vitreous in Sec. 2. For the computational model, low Peclet number limit is relaxed and moderate Pe values are admitted. The fluid flow in the vitreous is still considered incompressible. For momentum conservation, the Brinkman flow model is used so that the no-slip condition is effectively satisfied at the capsule surface. For mass-transport modeling, the classical convection-diffusion equation is used in the fully time-dependent form in both regions (within the capsule and outside).

3.3 Fluid Flow and Mass Transport Equations. The fluid in the vitreous is considered to be incompressible so that

$$\nabla^* \cdot \boldsymbol{u}^* = 0 \tag{106}$$

This is consistent with Eq. (1). For Darcy flow, the momentum equation is

$$\boldsymbol{u}^* = -\frac{K}{\mu}\nabla^* p^* \tag{107}$$

as stated in Eq. (1). In the case of Brinkman flow, the momentum equation is given by

$$\nabla^* \cdot (\tilde{\mu}\nabla^* \boldsymbol{u}^*) - \left(\frac{\mu}{K}\boldsymbol{u}^* + \nabla^* p^*\right) = 0 \tag{108}$$

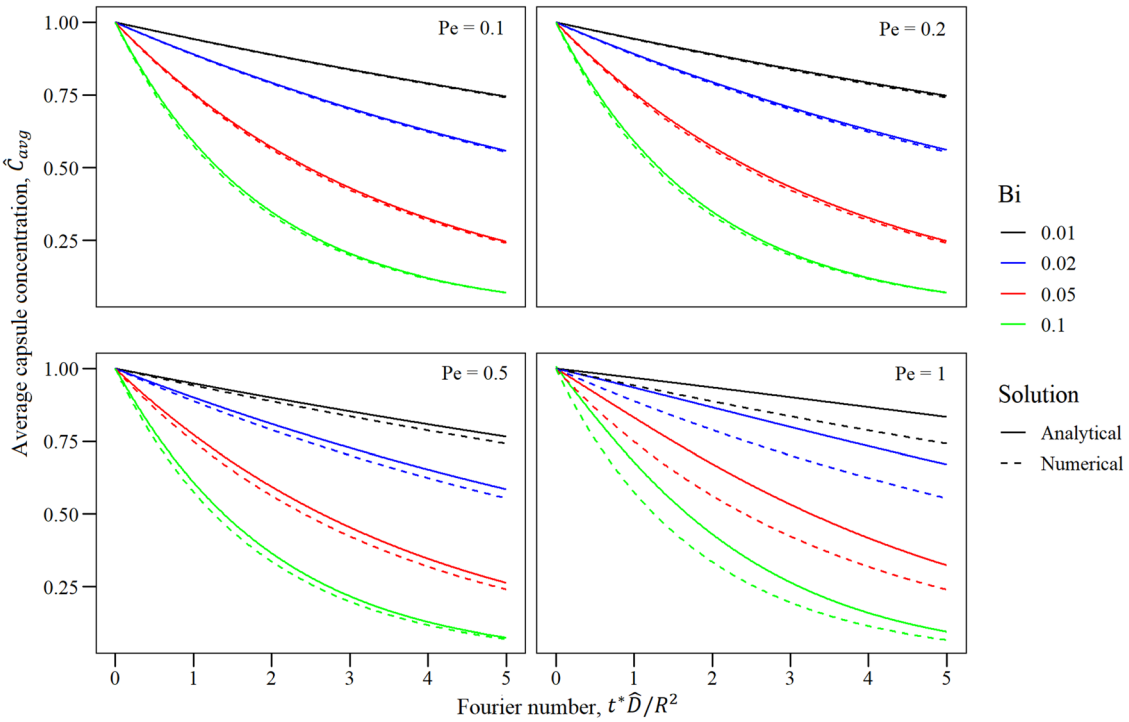

Fig. 7 Comparison of analytical and numerical solutions of average concentration

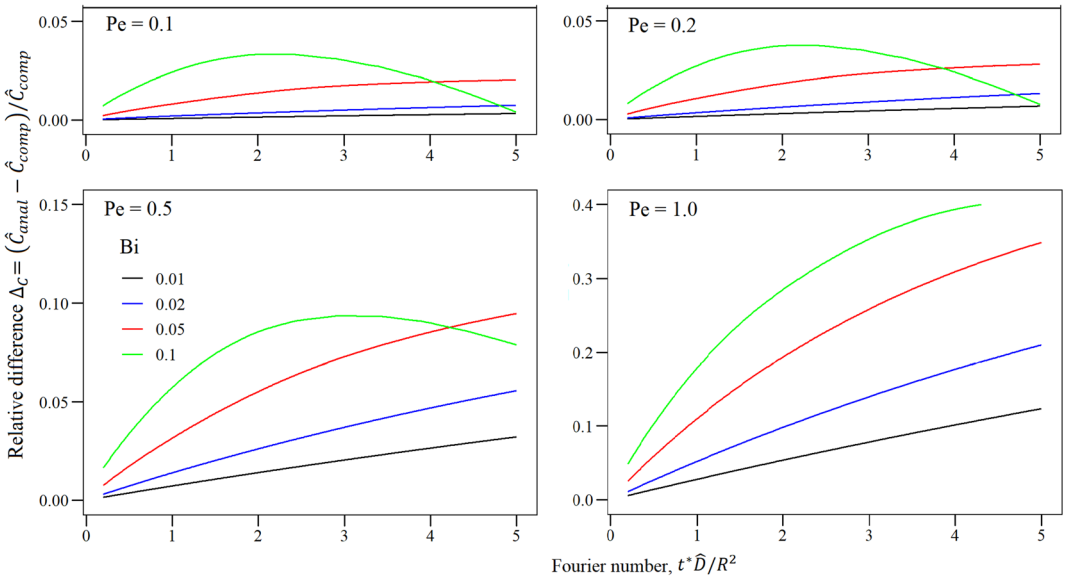

Fig. 8 Relative difference $\Delta_C = (\hat{C}_{anal} - \hat{C}_{comp})/\hat{C}_{comp}$ between analytical and computational results for the average concentration

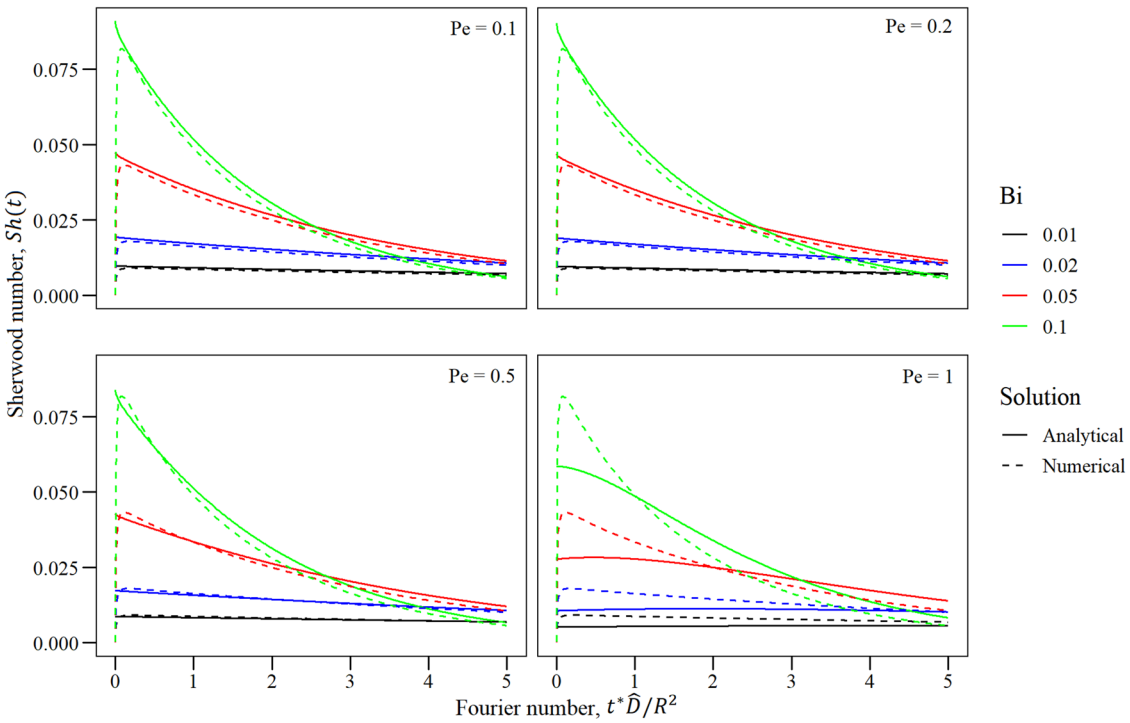

Fig. 9 Comparison of analytical and numerical solutions for the Sherwood number

where $\tilde{\mu}$ is a modified viscosity and the term therein applies near the boundary facilitating the no-slip condition. Thus, the boundary condition (5) is modified so that

$$\boldsymbol{u}^* \big|_{r^*=R} = 0 \tag{109}$$

For common porous media $\tilde{\mu} = \mu/\varepsilon'$ has been adopted [30] where ε' is the permeability. The mass transfer outside the capsule and inside is given by Eqs. (2) and (3), respectively. The other initial/boundary/interface conditions (4), and (6)–(9) apply as they are. Computationally, in place of (8), we apply the symmetry condition about the z-axis. For mass transfer simulation, no-penetration boundary condition is applied to the walls. At the inlet and the outlet, mixed boundary conditions are applied whereby the penetrating fluid carries the drug at its concentration level and membrane permeability coefficients l_i and l_o are applied. Some of these conditions are restated in Table 1 for the sake of completeness. It should be mentioned that since these interfaces are quite far removed from the main activity center (the capsule), the results are quite insensitive to l_i and l_o values.

4 Results and Discussion

4.1 Fluid Flow. The flow field from the computational analysis is presented in Fig. 6. The streamlines emanate from the hyaloid and terminate in the retina.

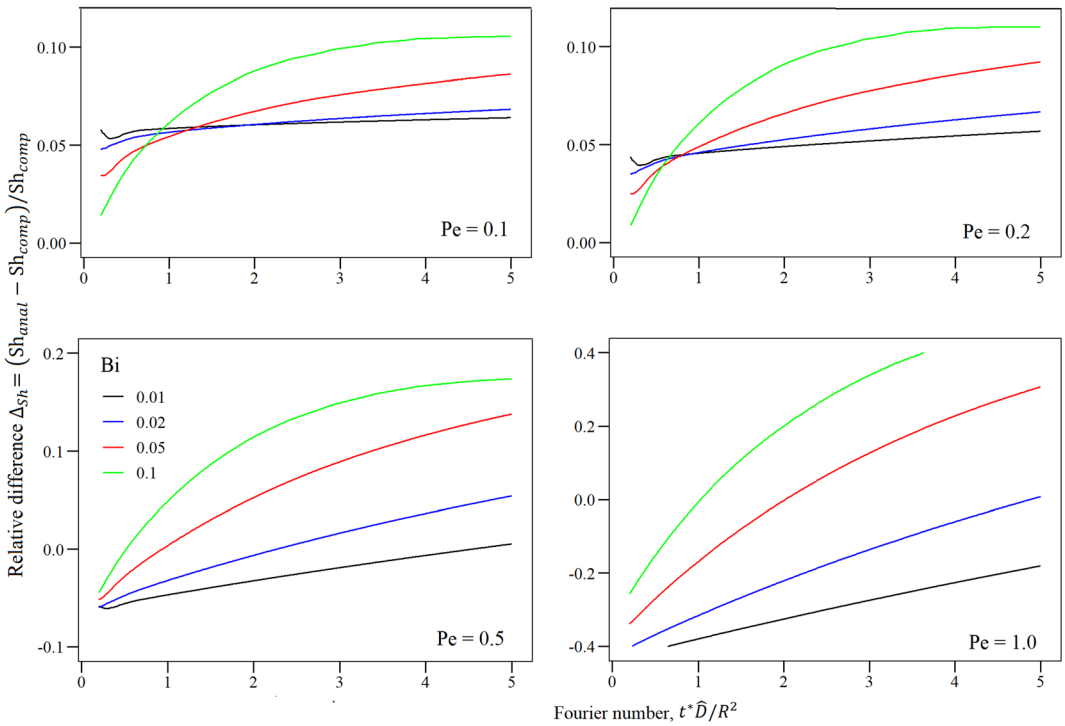

Fig. 10 Relative difference $\Delta_{Sh} = (Sh_{anal} - Sh_{comp})/Sh_{comp}$ between analytical and computational results for the Sherwood number

4.2 Mass Transfer Validation. The validation of the computational results is carried out by comparison with the perturbation analysis for $Pe \ll 1$. First, for the eye geometry, the flow field was obtained without the capsule. The flow velocity at the capsule location was obtained and applied as the far-field velocity U_0 in the perturbation analysis. It is this velocity that was used to determine the Peclet number. The analytical solution is derived for drug diffusion from a sphere into an infinite medium with Darcy flow past the sphere. Figures 7–10 present the comparisons of the numerical solutions with the analytical solution for different Peclet numbers and Biot numbers. Figure 7 corresponds to the solutions of the average concentration inside the sphere. The difference between the analytical and computational results is very small for Pe ≤ 0.2. Even for Pe $= 0.5$, the agreement is quite good. To see the relative difference between the analytical and the computational results, the parameter, $\Delta_C = (\widehat{C}_{\text{anal}} - \widehat{C}_{\text{comp}})/\widehat{C}_{\text{comp}}$, is calculated and plotted as a function of the Fourier number in Fig. 8 where the deviation is presented on a stretched vertical scale to amplify the differences. It should be noted that the vertical scale for Pe $= 1.0$, the scale is different from the lower values of Pe. Figure 9 corresponds to Sherwood number calculations in terms of Fourier number which represents the nondimensional time. As with the average capsule concentration results, the Sherwood number values agree very well small Peclet numbers (Pe ≤ 0.5). It is of course noticeable that the greater the Peclet number becomes, the higher the intercept offset between analytical and numerical solutions becomes. This is an expected observation because the analytical solution assumes small values of Peclet number and is valid only for those values. For Pe $= 1$, deviation between computational and analytical results is significant. To illustrate the deviation, we have plotted the relative deviation between these results $\Delta_{\text{Sh}} = (\text{Sh}_{\text{anal}} - \text{Sh}_{\text{comp}})/\text{Sh}_{\text{comp}}$ in Fig. 10. Once again, we point out that the vertical scales for the different Peclet numbers are not all the same.

Based on the aforementioned results and observation, it is concluded that the numerical method is valid and matches the analytical solution within the limits of low Peclet number assumptions. The computations were carried out for an axisymmetric system since the capsule is placed on the eye centerline. However, it is feasible to carry out fully 3D computations and we expect the localized flow perturbation analysis about the capsule to still hold.

5 Conclusions

For a sustained-release drug capsule, computational and analytical predictions have been carried for the drug release rate and the average capsule concentration. The analytical solution has been developed by a singular-perturbation procedure for Pe $\ll 1$. The analytical flow field is based on Darcy's equation with uniform surrounding flow in the local region around the capsule. We have the following conclusions for the computational and analytical models:

(1) The singular perturbation results with Peclet number Pe $= \varepsilon$ as a small parameter have been obtained to give the drug mass transfer rate from the capsule and the concentration of the remaining drug as a function of dimensionless time.
(2) The overall mass transfer is devoid of the angular-dependent terms since such terms integrate to zero over the surface of the sphere. The nonradial effect at $O(\varepsilon)$, however, brings a contribution to the purely radial part at $O(\varepsilon^2)$.
(3) The convective transport brings about the asymmetry that contributes to the overall mass transfer in the form of the Peclet number Pe $= \varepsilon$.
(4) The capsule membrane permeability (mass-transfer Biot number) is the controlling parameter and further limiting analysis for Bi $\ll 1$ followed by straightforward mass-transfer calculations gives the capsule half-life as $T_{1/2} = [(1 + \text{Bi})/3\text{Bi}]\ln 2$
(5) The computational model using Brinkman flow allows us to conform more closely to the eye geometry and provides drug transport to Pe $= O(1)$ and higher. We also see that the analysis based on the local flow in the vicinity of an isolated capsule is quite reasonable.

(6) The comparisons of the two models show excellent agreement at $\varepsilon = 0.1$ and lower values. The computational model shows somewhat slower release rate than the perturbation model. This owes largely to the quasi-steady model for the exterior-region transport.

Funding Data

- National Eye Institute (NEI) under NIH (Grant No. 5R01EY026599; Funder ID: 10.13039/100000053).

Nomenclature

Roman Symbols

$b = \mathrm{Bi}/(1+\mathrm{Bi})$
$\mathrm{Bi} = lR/D$ = mass-transfer Biot number
c = drug concentration
C = drug concentration, outer variable
$\widehat{C}_k(t)$ = average capsule concentration components
D = diffusion coefficient
$f_n(\varepsilon)$ = perturbation expansion parameter
$\mathrm{Fo} = t^*D/R^2$ = Fourier number
$g(\varepsilon)$ = perturbation expansion parameter
$G_n = 1 - \Phi_D + \Phi_D^2\lambda_n^2$
h_k = concentration (inner perturbation expansion)
H_k = concentration (outer perturbation expansion)
$i_n(\,), k_n(\,)$ = spherical Bessel functions
K = Darcy coefficient (permeability)
l = membrane permeability
$\mathcal{L}$ = Laplace transform operator
$\boldsymbol{n}$ = unit normal vector
p = pressure
P = dimensionless pressure
$P_n(\bar{\mu})$ = Legendre polynomials
$\mathrm{Pe} = \varepsilon$ = Peclet number
$\mathrm{q} = s^{1/2}$ = Laplace parameter
Q = total mass flow
$q_a^\delta(t), q_b^\delta(t), q_b^\lambda(t), q_b^\beta(t)$ = $\mathrm{Sh}_2(t)$ components
r = radial coordinate
R = capsule radius
s = Laplace domain variable
Sh = Sherwood number
t = time
$\boldsymbol{u}$ = velocity
U_0 = local velocity around capsule
z = vertical coordinate

Greek Symbols

β_n = transcendental function roots (Eq. (96))
δ_n = transcendental function roots (Eq. (95))
Δ = computational versus analytical relative difference
ε = perturbation parameter, Peclet number
$\eta = 1/Bi + \frac{1}{2}$
θ = angular coordinate
λ_n = transcendental function roots (Eq. (89))
μ = viscosity
$\tilde{\mu}$ = viscosity adjusted for Brinkman flow
$\bar{\mu} = \cos\theta$
$\rho = \varepsilon r$ = outer radial coordinate
$\phi_D = \widehat{D}/D$ = diffusion coefficients ratio
$\Phi_D = \phi_D(1 + 1/\mathrm{Bi})$
$\Psi_D = \phi_D\left(\frac{1}{2} + 1/\mathrm{Bi}\right)$

Subscripts/Superscripts

anal = analytical
C = in reference to concentration
comp = computational
i = inlet
o = outlet
Sh = in reference to Sherwood number
* = dimensioned variables
0,1,2,. = perturbation expansion hierarchy

Accents

$\widehat{\ }$ = capsule parameters
$\bar{\ }$ = overbar, Laplace transformed variables

References

[1] Lee, S., and Robinson, M., 2009, "Novel Drug Delivery Systems for Retinal Diseases. A Review," Ophthal. Res, **41**(3), pp. 124–135.
[2] Penkova, A., Moats, R., Humayun, M., Fraser, S., and Sadhal, S., 2019, "Diffusive Transport in the Vitreous Humor," ASME J. Heat Transfer-Trans. ASME, **141**(5), p. 050801.
[3] Penkova, A., Rattanakijsuntorn, K., Sadhal, S., Tang, Y., Moats, R., Hughes, P. M., Robinson, M. R., and Lee, S. S., 2014, "A Technique for Drug Surrogate Diffusion Coefficient Measurement by Intravitreal Injection," Int. J. Heat Mass Transfer, **70**(01), pp. 504–514.
[4] Lee, S. S., Hughes, P., Ross, A. D., and Robinson, M. R., 2010, "Biodegradable Implants for Sustained Drug Release in the Eye," Pharm. Res., **27**(10), pp. 2043–2053.
[5] Choonara, Y. E., Pillay, V., Danckwerts, M. P., Carmichael, T. R., and Du Toit, L. C., 2010, "A Review of Implantable Intravitreal Drug Delivery Technologies for the Treatment of Posterior Segment Eye Diseases," J. Pharm. Sci., **99**(5), pp. 2219–2239.
[6] Herrero-Vanrell, R., and Refojo, M. F., 2001, "Biodegradable Microspheres for Vitreoretinal Drug Delivery," Adv. Drug Deliv. Rev., **52**(1), pp. 5–16.
[7] Wang, J., Jiang, A., Joshi, M., and Christoforidis, J., 2013, "Drug Delivery Implants in the Treatment of Vitreous Inflammation," Mediators Inflamm., **2013**(01), pp. 1–8.
[8] Yasukawa, T., Ogura, Y., Kimura, H., Sakurai, E., and Tabata, Y., 2006, "Drug Delivery From Ocular Implants," Expert Opin. Drug Deliv., **3**(2), pp. 261–273.
[9] Ferreira, J., Gonçalves, M., Gudiño, E., Maia, M., and Oishi, C., 2020, "Mathematical Model for Degradation and Drug Release From an Intravitreal Biodegradable Implant," Comput. Math. Appl., **80**(10), pp. 2212–2240.
[10] Rodrigues da Silva, G., Ligório Fialho, S., Camargo Siqueira, R., Jorge, R., and da Silva Cunha Júnior, A., 2010, "Implants as Drug Delivery Devices for the Treatment of Eye Diseases," Braz. J. Pharm. Sci., **46**(3), pp. 585–595.
[11] Bourges, J., Bloquel, C., Thomas, A., Froussart, F., Bochot, A., Azan, F., Gurny, R., Benezra, D., and Behar-Cohen, F., 2006, "Intra-Ocular Implants for Extended Drug Delivery: Therapeutic Applications," Adv. Drug Deliv. Rev, **58**(11), pp. 1182–1202.
[12] Chandra, R., and Rustgi, R., 1998, "Biodegradable Polymers," Prog. Polym. Sci, **23**(7), pp. 1273–1235.
[13] Charles, N., and Steiner, G., 1996, "Ganciclovir Intra-Ocular Implant. A Clinicopathologic Study," Ophthalmology, **103**(3), pp. 416–421.
[14] Fialho, S., Behar-Cohen, F., and Silva-Cunha, A., 2008, "Dexamethasone-Loaded Poly(e-Caprolactone) Intravitreal Implants: A Pilot Study," Eur. J. Pharm. Biopharm, **68**(3), pp. 637–646.
[15] Kimura, H., and Ogura, Y., 2001, "Biodegradable Polymers for Ocular Drugs Delivery," Ophthalmologica, **215**(3), pp. 143–155.
[16] Kunou, N., Ogura, Y., Hashizoe, M., Honda, Y., Hyon, S., and Ikada, Y., 1995, "Controlled Intra-Ocular Delivery of Ganciclovir With Use of Biodegradable Scleral Implant in Rabbits," J. Control. Release, **37**(1–2), pp. 143–150.
[17] Smith, T., Pearson, P., Blandford, D., Brown, J., Goins, K., Hollins, E., Schmeisser, E., Glavinos, P., Baldwin, L., and Ashton, P., 1992, "Intravitreal Sustained-Release Ganciclovir," Arch. Ophthalmol, **110**(2), pp. 255–258.
[18] Yasukawa, T., Ogura, Y., Sakurai, E., Tabata, Y., and Kimura, H., 2005, "Intraocular Sustained Drug Delivery Using Implantable Polymeric Devices," Adv. Drug Deliv. Rev, **57**(14), pp. 2033–2046.
[19] Kim, H., Lizak, M. J., Tansey, G., Csaky, K. G., Robinson, M. R., Yuan, P., Wang, N. S., and Lutz, R. J., 2005, "Study of Ocular Transport of Drugs Released From an Intravitreal Implant Using Magnetic Resonance Imaging," Ann. Biomed. Eng., **33**(2), pp. 150–164.
[20] Penkova, A. N., Zhang, S., Humayun, M. S., Fraser, S., Moats, R., and Sadhal, S. S., 2020, "Measurement of the Hydraulic Conductivity of the Vitreous Humor," J. Porous Media, **23**(2), pp. 195–206.
[21] Sebag, J., 1992, "The Vitreous," *Adler's Physiology of the Eye*, W. M. Hart, ed., 9th ed., Mossby, Inc, St Louis, MO, pp. 268–347.
[22] Dehdashti, E., and Masoud, H., 2020, "Forced Convection Heat Transfer From a Particle at Small and Large Peclet Numbers," ASME J. Heat Transfer-Trans. ASME, **142**(6), p. 061803.
[23] Feng, Z.-G., 2013, "Forced Heat and Mass Transfer From a Slightly Deformed Sphere at Small but Finite Peclet Numbers in Stokes Flow," ASME J. Heat Transfer-Trans. ASME, **135**(8), p. 081702.

[24] Goddard, J., and Acrivos, A., 1967, "An Analysis of Laminar Forced-Convection Mass Transfer With Homogeneous Chemical Reaction," Q. J. Mech. Appl. Math., **20**(4), pp. 471–497.
[25] Acrivos, A., and Goddard, J., 1965, "Asymptotic Expansions for Laminar Forced-Convection Heat and Mass Transfer," J. Fluid Mech., **23**(02), pp. 273–291.
[26] Acrivos, A., and Taylor, T. D., 1962, "Heat and Mass Transfer From Single Spheres in Stokes Flow," Phys. Fluids, **5**(4), pp. 387–393.
[27] Gupalo, Y. P., and Ryazantsev, Y. S., 1972, "Mass and Heat Transfer From a Sphere in a Laminar Flow," Chem. Eng. Sci., **27**(1), pp. 61–68.
[28] Bell, C. G., Byrne, H. M., Whiteley, J. P., and Waters, S. L., 2013, "Heat or Mass Transfer From a Sphere in Stokes Flow at Low Péclet Number," Appl. Math. Lett., **26**(4), pp. 392–396.
[29] Sadhal, S. S., 1993, "Transient Heat Transfer From a Solid Sphere Translating at Low Reynolds Number: A Perturbation Solution at Low Peclet Number," Heat Mass Transfer, **28**(6), pp. 365–370.
[30] Liu, S., and Masliyah, J. H., 2005, "Dispersion in Porous Media," *Handbook of Porous Media*, K. Vafai, ed., 2nd ed., Taylor & Francis Group, Boca Raton, FL, pp. 81–140.